Eur. Phys. J. E **4**, 33–43 (2001)

THE EUROPEAN PHYSICAL JOURNAL E

EDP Sciences

Local entropic effects of polymers grafted to soft interfaces

T. Bickel[1], C. Jeppesen[2], and C.M. Marques[1]

[1] L.D.F.C.-UMR 7506, 3 rue de l'Université, 67084 Strasbourg Cedex, France
[2] Materials Research Laboratory, University of California, Santa Barbara, CA 93106, USA

Received 20 April 2000

Abstract. In this paper, we study the equilibrium properties of polymer chains end-tethered to a fluid membrane. The loss of conformational entropy of the polymer results in an inhomogeneous pressure field that we calculate for Gaussian chains. We estimate the effects of excluded volume through a relation between pressure and concentration. Under the polymer pressure, a soft surface will deform. We calculate the deformation profile for a fluid membrane and show that close to the grafting point, this profile assumes a cone-like shape, independently of the boundary conditions. Interactions between different polymers are also mediated by the membrane deformation. This pair-additive potential is attractive for chains grafted on the same side of the membrane and repulsive otherwise.

PACS. 36.20.-r Macromolecules and polymer molecules – 87.15.He Dynamics and conformational changes – 87.16.Dg Membranes, bilayers, and vesicles.

1 Introduction

Fluid membranes are surfactant bilayers self-assembled from solution [1]. They are the prevalent constituents of many natural and industrial colloidal suspensions, that often contain also other macromolecular species. In the biological realm, phospholipid bilayers build the walls of liposomes and cells, hosting proteins responsible for functions as diverse as anchoring the cytoskeleton, providing coating protection against the body immune response or opening ionic channels for osmotic compensation [2]. In cosmetics, pharmaceutics or detergency, many formulations are membrane solutions with polymers added for performance, processing, conditioning or delivery [3].

The interactions between polymers and fluid bilayers have been well scrutinized in many systems. Polymers grafted to the bilayers can induce gelation [4] or other phase changes [5,6] in liquid lamellar phases. They stabilize monodisperse vesicles [7] and modify the geometry of monolamellar [8,9] and multilamellar cylindrical vesicles [10]. Theoretically, the behaviour of fluid membranes is well understood in terms of bending elasticity [11,12], a description that requires as an input the value of three material constants: the bending rigidity κ, the Gaussian rigidity $\bar{\kappa}$ and the spontaneous curvature radius R_0. One might hope that the behaviour of mixed systems can still be described by an effective elastic energy, with modified material constants. The task that theoretical studies have undertaken is to calculate the modifications induced on κ, $\bar{\kappa}$ and R_0 by the addition of the macromolecules [13–17].

However, polymer-membrane interactions must have a local quality. For instance, if a polymer is end-tethered to a membrane, it is clear that the interactions are strong at the anchoring point and vanish far enough from it. We show in this paper that, for grafted polymers, it is possible to construct a local description of polymer membrane interactions. Our description stands on the recognition that an end-grafted polymer applies a pressure field to the grafting wall [18,19]. The pressure field results into a local deformation of the membrane: a membrane with grafted polymers can therefore be seen as a surface with bending elasticity carrying a number of pressure patches, each of them creating its own deformation.

The paper is organized as follows. In the next section we compute the pressure field applied by a grafted polymer in theta and good solvent conditions. In Section 3, we consider the case of a freely standing membrane, for which we compute the deformation induced by the polymer pressure patch. We also show in this section that the interactions between the different deformation fields give rise to a membrane-mediated potential between different grafted polymers. The consequences of such potential are briefly discussed. Section 4 is dedicated to two membrane geometries relevant for experiments. We first discuss the case of supported membranes, and then the case of lamellar phases. In the conclusions, we will briefly speculate on the implications of our results for hairy vesicles.

2 The pressure applied by a grafted polymer

The number of available conformations for a long, flexible polymer is strongly reduced by the process of end-grafting the chain to a hard wall [20,21]. The average

configuration of the macromolecule is a compromise between the need to avoid the surface and the constraint imposed by the tethered end. It is clear that if the surface can be deformed, there will be an entropic reason to push it away from the monomer cloud. This can be described as a pressure that the polymer applies to the grafting wall. In the following paragraph we explicitly compute the pressure for ideal chains and relate it to the concentration at the wall. We then argue that this also provides a good pathway to compute the pressure applied by chains with excluded volume.

2.1 Gaussian grafted chain

We consider a Gaussian chain of N units, end-tethered by one extremity to a non-adsorbing wall. The surface is described by its height $h(x,y)$, where (x,y) denotes the position in the horizontal coordinates frame. The thermodynamic properties of the chain are described by the propagator $G_N(\mathbf{r},\mathbf{r}')$, that satisfies the Edwards equation [22]

$$\frac{\partial G_N(\mathbf{r},\mathbf{r}')}{\partial N} = \frac{a^2}{6}\Delta G_N(\mathbf{r},\mathbf{r}') \tag{1}$$

with the following boundary conditions: $G_N(\mathbf{r},\mathbf{r}') \equiv 0$ on the wall and $\lim_{N\to 0} G_N(\mathbf{r},\mathbf{r}') = \delta(\mathbf{r}-\mathbf{r}')$. The length a is the monomer size. The statistical weigth of the chain attached at a monomer distance from the origin $\mathbf{a} = (0,0,a)$ is given by

$$Z_N(\mathbf{a}) = \int \mathrm{d}\mathbf{r}'\, G_N(\mathbf{a},\mathbf{r}'), \tag{2}$$

the integral running over all the space available for the free end. In the flat, reference case $h(x,y) = 0$, the Green function can be factorized:

$$G_N^{(0)}(\mathbf{r},\mathbf{r}') = (\tfrac{3}{2\pi N a^2})^{3/2} \exp\{-\tfrac{3(x-x')^2}{2Na^2}\} \exp\{-\tfrac{3(y-y')^2}{2Na^2}\} \times(\exp\{-\tfrac{3(z-z')^2}{2Na^2}\} - \exp\{-\tfrac{3(z+z')^2}{2Na^2}\}) \tag{3}$$

and the partition function is

$$Z_N^{(0)}(\mathbf{a}) = \int_{-\infty}^{+\infty}\mathrm{d}x' \int_{-\infty}^{+\infty}\mathrm{d}y' \int_0^{+\infty}\mathrm{d}z'\, G_N^{(0)}(\mathbf{a},\mathbf{r}') = \mathrm{erf}\left(\frac{a}{2R_\mathrm{g}}\right) \tag{4}$$

with $R_\mathrm{g} = \sqrt{Na^2/6}$ the gyration radius of the chain, and erf the error function [23]. Now we seek for a perturbative solution [24] of the Edwards equation by performing a small displacement h of the surface. We write the partition function as $Z_N = Z_N^{(0)} + Z_N^{(1)} + Z_N^{(2)} + \ldots$, where $Z_N^{(i)}$ is of order h^i and $Z_N^{(0)}$ is defined in equation (4). One can notice that due to the linearity of equation (1), each term of the perturbative expansion obeys an Edwards equation

$$\frac{\partial Z_N^{(i)}}{\partial N} = \frac{a^2}{6}\Delta Z_N^{(i)}\ , \qquad i = 0,1,2,\ldots\ . \tag{5}$$

The solutions of successive orders are coupled through the boundary conditions on the wall:

$$\begin{aligned} 0 &= Z_N(x,y,h) \\ &= Z_N(x,y,0) + h(x,y)\frac{\partial Z_N}{\partial z}(x,y,0) \\ &\quad + \frac{h^2(x,y)}{2}\frac{\partial^2 Z_N}{\partial z^2}(x,y,0) + \ldots\ . \end{aligned} \tag{6}$$

In the following, we concentrate on the first-order term $Z_N^{(1)}$, that is related, as we will see, to the pressure exerted by the polymer on the surface. $Z_N^{(1)}$ is given by the solution of equation (5) with the boundary condition

$$Z_N^{(1)}(x,y,0) = -h(x,y)\frac{\partial Z_N^{(0)}}{\partial z}(x,y,0). \tag{7}$$

The solution can then be written as [25]

$$Z_N^{(1)}(\mathbf{a}) = \frac{a^2}{6}\int_0^N \mathrm{d}n \int \mathrm{d}S\, \frac{\partial G_{N-n}^{(0)}}{\partial z}(x,y,0;\mathbf{a})\, Z_n^{(1)}(x,y,0) \tag{8}$$

so that the displacement of the surface is achieved to first order in h by the work

$$\begin{aligned} \Delta F &= F[h] - F[0] \\ &= -k_\mathrm{B}T \log\left[1 + \frac{Z_N^{(1)}}{Z_N^{(0)}}\right] \\ &= \int \mathrm{d}S p(x,y)h(x,y), \end{aligned} \tag{9}$$

where the function $p(x,y)$ has the radially symetric form

$$p(r) = \frac{k_\mathrm{B}T}{2\pi(r^2+a^2)^{3/2}}\left(1 + \frac{r^2+a^2}{2R_\mathrm{g}^2}\right)\exp\left\{-\frac{r^2+a^2}{4R_\mathrm{g}^2}\right\} \tag{10}$$

with $r = \sqrt{x^2+y^2}$. At point $\mathbf{r} = (x,y)$, the elementary work $\mathrm{d}F$ required to displace a volume $\mathrm{d}V(r) = h(r)\mathrm{d}S$ is given by $\mathrm{d}F = p(r)h(r)\mathrm{d}S$. The function $p(r)$ is therefore the pressure applied by the polymer on the surface at point r. It is a non-homogeneous function —see Figure 1— that sharply decays from its maximum value at the anchoring point with the scaling form

$$p(r) \simeq \frac{k_\mathrm{B}T}{2\pi r^3} \text{ for } a \ll r \ll R_\mathrm{g}. \tag{11}$$

Well inside the polymer umbrella ($a \ll r \ll R_\mathrm{g}$), where the only relevant length is r, expression (11) is the natural scaling for the pressure. In this region, most of the monomers that contribute to the pressure are close to the grafted end. For distances larger than the polymer size, the pressure vanishes exponentially. A grafted polymer can then be pictured as a microscopic pressure tool that applies a well-defined but non-homogeneous force on a disk of radius $\sim 2R_\mathrm{g}$ centered at the anchoring position. In the middle of the patch the pressure has a strong value: $p(0) \simeq 2.4 \times 10^7$ Pa for $a = 0.3$ nm at room temperature

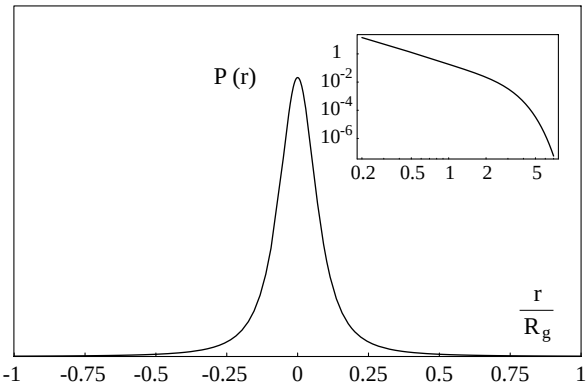

Fig. 1. The pressure applied by a grafted polymer to the surface. We chose here $a = 0.1R_{\rm g}$ and arbitrary units of pressure. The insert stresses the scaling form r^{-3} close to the grafting point.

$T = 25°$C. A small area within a monomer distance from the origin supports most of the total force f exerted by the chain onto the surface

$$f = \int_0^\infty 2\pi r {\rm d}r p(r) = \frac{k_{\rm B}T}{a} \exp\left(-\frac{a^2}{4R_{\rm g}^2}\right) \simeq 13.3 \text{ pN}, \tag{12}$$

with the precedent values of monomer size and temperature. The grafted monomer exerts a point-like force $-f$ that ensures mechanical equilibrium.

Previous work [15,26] has focused on curvature contributions to the polymer free energy ΔF: by considering a surface of a given shape, ΔF is calculated as a function of the curvature $\frac{1}{R}$. For instance, for a sphere and a cylinder one gets $\Delta F_{\rm sph} = -\sqrt{\pi} k_{\rm B}T \frac{R_{\rm g}}{R}$ and $\Delta F_{\rm cyl} = \frac{1}{2}\Delta F_{\rm sph}$. The minus sign indicates that the energy is lowered by spherical and cylindrical surfaces that bend away from the polymer. We naturally recover these results by considering a general surface defined by $h(x,y) = -\frac{x^2}{2R_1} - \frac{y^2}{2R_2}$, and evaluating the integral (9) with $R_1 = R_2 = R$ for a sphere and $R_1 = R$, $R_2 = 0$ for a cylinder. Interestingly, for a minimal surface ($R_1 = -R_2 = R$), there is no contribution of the curvature to the free energy ($\Delta F = 0$): to first order, the entropic cost of tethering a Gaussian chain to a plane or to a minimal surface is the same.

2.2 Relation between pressure and concentration

As explained above, the pressure that a grafted polymer exerts on the wall has an entropic origin: by displacing the surface at point $\mathbf{r} = (x, y)$ from its flat position $h(\mathbf{r})$ one increases ($h < 0$) or decreases ($h > 0$) the number of allowed chain configurations. The work per unit surface associated with the corresponding entropy gain or loss defines the pressure. Alternatively, the pressure can be viewed as resulting from the forces applied by all the monomers at a given surface point. If the surface potential acting on each monomer is $u(z)$, the pressure is given by [27]

$$p(x,y) = -\int_0^\infty {\rm d}z \frac{\partial u}{\partial z}(z) c(x,y,z) \tag{13}$$

with c the monomer concentration. Expression (13) reveals the linear relationship between pressure and concentration at the wall but is not very useful for the continuous Gaussian chain considered in this paper. Instead, we directly derive the pressure-concentration relation by noting that the monomer concentration of a chain tethered to a flat surface is written as [20]

$$c^{(0)}(\mathbf{r}) = \frac{1}{Z^{(0)}(\mathbf{a})} \int_0^N {\rm d}n G_n^{(0)}(\mathbf{a}, \mathbf{r}) Z_{N-n}^{(0)}(\mathbf{r}). \tag{14}$$

The interaction with the wall being purely repulsive, one has $c^{(0)}(x,y,0) = 0$ and $\frac{\partial c^{(0)}}{\partial z}(x,y,0) = 0$, the second derivative of the concentration being the lowest derivative that does not vanish on the surface. Rewriting more explicitly equation (8) leads to

$$Z_N^{(1)}(\mathbf{a}) = -\tfrac{a^2}{6} \int {\rm d}S\, h(x,y) \int_0^N {\rm d}n \frac{\partial G_n^{(0)}}{\partial z}(\mathbf{a}; x, y, 0) \times \frac{\partial Z_{N-n}^{(0)}}{\partial z}(x,y,0), \tag{15}$$

so that we directly deduce from (9) and (14) the relation

$$p(r) = k_{\rm B}T \frac{a^2}{12} \frac{\partial^2 c^{(0)}}{\partial z^2}(r, 0) \tag{16}$$

with $r = \sqrt{x^2 + y^2}$. Qualitatively, the pressure can be associated with an ideal gas pressure caused by the concentration of monomers at a distance $z = \frac{a}{\sqrt{6}}$ from the wall:

$$p(r) = k_{\rm B}T c^{(0)}\left(r, z = \frac{a}{\sqrt{6}}\right). \tag{17}$$

Equivalently, equation (13) can be used to assert that the effective wall potential acting on the monomers has a second moment of forces given by $\int_0^\infty {\rm d}z z^2 \frac{\partial u}{\partial z}(z) = k_{\rm B}T \frac{a^2}{6}$.

2.3 Grafted self-avoinding walks

Flexible polymer chains in good solvent cannot be described by Gaussian statistics. They only exhibit ideal Gaussian behaviour close to the theta temperature, at which monomer attraction compensates for steric repulsion. Above the theta point, the polymers perform self-avoiding walks (SAWs) which lead to distinct statistics. In particular, the average dimension of a SAW coil is larger than its Gaussian equivalent, the end-to-end distance scales as $R = N^\nu a$, with ν the Flory exponent, close to $\nu \simeq 3/5$.

As stated in equation (13), the proportionality between the polymer pressure and the monomer concentration in the vicinty of the wall is expected to hold on general grounds, independently of the approximations involved. Altough equation (13) does not easily provide for

a proportionality coefficient, it does give a firm ground for predicting the scaling form of the pressure applied to the wall by grafted chains in a good solvent. For comparison, we first recall the structure of the monomer concentration profile for a Gaussian grafted polymer, a case where an explicit calculation can be performed [21]. The cone of equation $z = r$ separates two regions in space. Outside the cone ($z \ll r$) but well inside the polymer "umbrella" ($z, r \ll R_g$), the monomer concentration grows quadratically from the wall, $c(r,z) \sim z^2/(r^3a^2)$. In this region the wall has an important depletion effect on the polymer configurations. Inside the cone ($z \gg r$) one recovers the usual bulk concentration of a Gaussian chain, $c(R) \sim 1/(Ra^2)$, where $\mathbf{R} = (\mathbf{r}, z)$ denotes the position in bulk. The crossover between the two behaviours occurs as one crosses the cone surface $z = r$. In the presence of excluded-volume interactions, the bulk concentration is given by $c(R) \sim 1/(R^{4/3}a^{5/3})$. For chains with excluded volume, the profile grows from the wall as $c(r,z) \sim z^{5/3}$. Writing the scaling form in the region $z \ll r$ that matches bulk behaviour at $z = r$ leads to $c(r,z) \sim z^{5/3}/(r^3a^{5/3})$. The pressure applied by a swollen grafted chain is therefore given by $p(r) \sim k_B T c(r, z = a) \sim k_B T r^{-3}$. It has the same scaling form as the pressure applied by ideal chains. We expect such scaling to be rather independent of the molecular details or of the differences between chain models.

Excluded-volume effects might nevertheless modify the amplitude and the range of the applied forces. In order to quantify these effects we implemented a Monte Carlo simulation on a polymer attached to a flat, impenetrable wall. The chain is described as a pearl necklace [28], each pearl of size a. The first monomer is grafted to the wall with center-of-mass position $(0,0,0)$. During simulation a histogram $c(r,z)$ for the monomer center-of-mass concentration at a distance r along the wall and height z above the wall is compiled. Although simulations are performed in a continuum, we calculate the concentration by discretizing space with a binsize of $0.18 \cdot a$ in the r and z direction. To extract the concentration at the wall at a distance r away from the grafting point we fit the function $f(z) = c(r,z)$ with a fourth-order polynomial in z multiplied with an exponential $\exp(-\lambda z)$, λ a fitting parameter. Upon extrapolating the fitted function to $z = 0$ we get the concentration of monomers at the wall at a given distance r: $\lim_{z\to 0} c(r,z)$. To ensure a reasonable error bar on the resulting concentration we generated $6 \cdot 10^6$ configurations for Gaussian random walks and self-avoiding random walks. By analysing the statistics for end-to-end distance, which represents the slowest relaxing mode for the chain, we estimate that we have an maximal error bar of 12% as r is increased from a few a, where the error bar is less, to $30 \cdot a$.

We first consider the Monte Carlo results for a chain without excluded volume. Because our Monte Carlo chain is actually a freely hinged chain, we do not expect the amplitude coefficient of the Gaussian model to exactly hold. We therefore plot in Figure 2a, both the expression for the pressure from equation (10) and the values for the monomer concentration at the wall extracted from a Monte Carlo simulation of a chain with $N = 200$ monomers. Agreement is excellent, except at distances of the order of a monomer size where the fixed length between monomers induces oscillations reminiscent of those observed in the correlation function of hard spheres. In Figure 2b we show equivalent results for a chain of $N = 200$ monomers with excluded volume. Agreement is also excellent, if we replace the dimension of the chain $R^2 = Na^2$ in expression (10) by $R^2 = 1.5N^{2\nu}a^2$, with $\nu = 0.6$. For the chain representation used in our simulations, excluded-volume effects influence only the range of the pressure field. The scaling form at small distances and even the amplitudes are equivalent to those of the ideal chains.

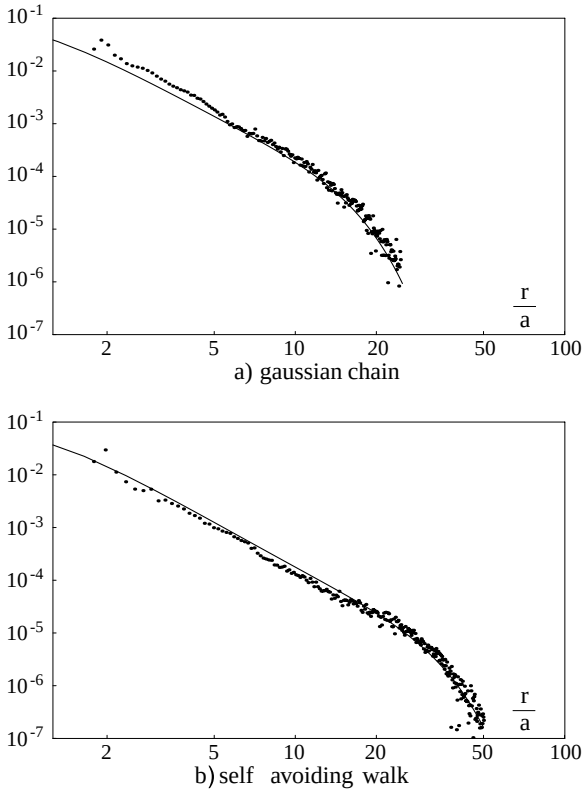

Fig. 2. Comparison of the calculated pressure and monomer concentration at the wall extracted from Monte Carlo simulations. a) Freely hinged chain of 200 monomers. b) Freely hinged chain of 200 monomers with excluded volume. The continuous line is the expression (16) of the pressure. Note that there is no adjustable parameter for the Gaussian chain. For the chain with excuded volume, the size of the polymer is $R^2 = 1.5N^{2\nu}a^2$, with $\nu = 0.6$.

3 Polymers anchored on a freely standing membrane

Grafted polymers are small pressure patches: when a polymer is grafted to a soft interface, the pressure deforms the interface into a characteristic shape which is determined

by the balance between the pressure and the elastic response of the grafting surface. In this chapter we consider first the deformation induced by a chain grafted on a freely standing elastic membrane, and then membrane-induced interactions between two grafted chains.

3.1 Deformation induced by the pressure field of a Gaussian polymer

The thermodynamic properties of a fluid membrane are well described by the Canham-Helfrich Hamiltonian [11], provided that the thickness d of the bilayer is small compared to the other relevant lengths of the problem (*i.e.* $d \ll R_{\rm g}$). The surface is described by its height $h(x,y)$, where $\mathbf{r} = (x,y)$ refers to the coordinate frame in the reference plane $h(x,y) = 0$. Assuming a gentle surface deformation ($\mid \nabla h \mid \ll 1$), the Hamiltonian is written in the Monge representation as

$$H = \frac{\kappa}{2} \int {\rm d}x{\rm d}y (\Delta h)^2 \tag{18}$$

with κ the bending rigidity and Δ the 2-dimensional Laplacian operator. For a membrane with fixed topology, the Gauss-Bonnet theorem implies that the Gaussian curvature term is constant and can therefore be ignored. For a purely repulsive surface, the total free energy of the system {membrane + polymer} is the sum of the bending energy of the membrane and the work of the entropic force exerted by the polymer

$$F[h] = F[0] + \frac{\kappa}{2} \int 2\pi r {\rm d}r (\Delta_r h)^2 + \int 2\pi r {\rm d}r p(r) h(r) \tag{19}$$

with $F[0]$ the work required to graft the polymer to a flat plane. Since both the applied pressure and the boundary conditions considered below are radially symmetric, we coveniently expressed all quantities in cylindrical coordinates. The equilibrium shape of the membrane ensues from a compromise between the applied pressure and the restoring bending forces. Functional minimization of the free energy with respect to the membrane profile $h(r)$ leads to the Euler-Lagrange equation for the equilibrium shape:

$$\kappa \Delta_r \Delta_r h(r) + p(r) = 0, \tag{20}$$

where $\Delta_r = \frac{1}{r}\frac{\rm d}{{\rm d}r} r \frac{\rm d}{{\rm d}r}$ is the radial part of the Laplacian operator. We first focus on the central region, close to the grafting point, where most of the stress is concentrated. Here ($r \ll R_{\rm g}$), the pressure behaves like $k_{\rm B}T/(2\pi r^3)$, so that the resulting deformation has a cone shape:

$$h(r) \underset{r\to 0}{\simeq} -\left(\frac{k_{\rm B}T}{\kappa}\right) \frac{r}{2\pi} \tag{21}$$

independently of the boundary conditions. A point-like defect is generated at the origin and we will refer to this conic shape as the *fundamental pinch* —see Figure 3. The surface curvature diverges at short distances as $\Delta_r h \propto r^{-1}$. Physically, this divergence is cut off either at a distance of the order of the membrane thickness d by non-harmonic terms in the curvature energy or, for infinitely thin membranes, at the monomer length a at which the pressure saturates. It is interesting to note that if a polymer is grafted to the tip of a purely conic deformation with an arbritary slope, and then the slope determined by balancing the *global* entropy gain of the polymer and the elastic cost of deforming the membrane into a cone shape, one finds the same slope as that of expression (21), given by the *local* balance of equation (20) [16]. This is an indication that the conic region supports most of the total stress imposed by the pressure patch. Neglecting effects in the cut off region, the analytical solution of equation (20) can be written as $h(r) = h_{\rm p}(r) + h_{\rm bh}(r)$, with $h_{\rm bh}(r) = \frac{k_{\rm B}T}{2\pi\kappa}[c_1 + c_2 \ln(r) + c_3 r^2 + c_4 r^2 \ln(r)]$ the kernel of the biharmonic operator and

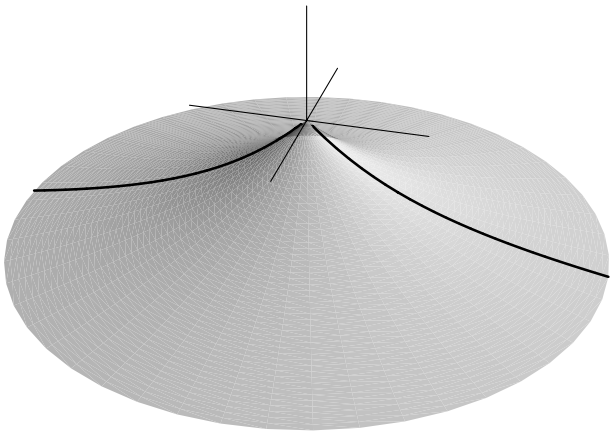

Fig. 3. The pinched form of a fluid membrane under the pressure of a grafted polymer. The deformation profile is the actual calculated form for a freely standing membrane.

$$h_{\rm p}(r) = -\frac{k_{\rm B}T}{2\pi\kappa}\left[\frac{1}{4} r \exp\left(-\frac{r^2}{4R_{\rm g}^2}\right) - \frac{\sqrt{\pi}}{8}\frac{r^2}{R_{\rm g}} {\rm erfc}\left(\frac{r}{2R_{\rm g}}\right) + \frac{\sqrt{\pi}}{4} R_{\rm g} {\rm erf}\left(\frac{r}{2R_{\rm g}}\right) + \frac{R_{\rm g}\sqrt{\pi}}{2}\int_0^{\frac{r}{R_{\rm g}}} \frac{{\rm d}u}{u} {\rm erf}\left(\frac{u}{2}\right)\right] \tag{22}$$

a particular solution of equation (20). The constants c_1, c_2, c_3 and c_4 are determined by the boundary conditions. In the simple case considered here, the membrane has no imposed constraints other than its known position of the center of coordinates $h(0) = 0$. Because there are no forces acting on the membrane at large distances from the center the average curvature must vanish there $\Delta_r h(r \to \infty) = 0$. This determines the four constants $c_1 = c_2 = c_3 = c_4 = 0$. At distances larger than $R_{\rm g}$, the profile is a catenoid, a radially symetric shape with zero average curvature,

$$h(r) \simeq -\frac{k_{\rm B}T}{2\pi\kappa} R_{\rm g} \ln\left(\frac{r}{R_{\rm g}}\right) \text{ for } r \gg R_{\rm g}. \tag{23}$$

The complete profile is displayed in Figure 3. It has a characteristic pinched shape, with a cone-like deformation

(20) that crosses over to the catenoidal shape (23). The divergence of the profile is related to the unconstrained nature of the membrane considered here. We will discuss in Section 4 how the deformation profile is modified by the boundary conditions or other external fields.

3.2 Interaction potential between two grafted polymers

Most often, bilayers anchor a finite concentration of polymers. Each polymer is a pressure patch that carries with it a pinched form. Beyond the usual Van der Waals or steric interactions between the different chains, the superimposition of the different pinches will also lead to membrane-mediated forces. Due to the linear nature of the pressure contribution to the free-energy of the system, the many-body problem reduces in this case to a sum of two-body interactions that we now study. Notice however that higher-order terms in the perturbative expansion would generate many-body interactions, but this point is far beyond the scope of this paper.

The free energy of two pressure patches applied at positions $\mathbf{r}_1$ and $\mathbf{r}_2$, *on the same side* of a membrane is

$$F[h,\mathbf{r}_1,\mathbf{r}_2] = \int \mathrm{d}S[p(\mid \mathbf{r}-\mathbf{r}_1 \mid)+p(\mid \mathbf{r}-\mathbf{r}_2 \mid)]h(\mathbf{r}) + \frac{\kappa}{2}\int \mathrm{d}S(\Delta h(\mathbf{r}))^2, \quad (24)$$

so that the deformation field obeys

$$\kappa\Delta\Delta h(\mathbf{r}) + p(\mid \mathbf{r}-\mathbf{r}_1 \mid)+p(\mid \mathbf{r}-\mathbf{r}_2 \mid) = 0 \quad (25)$$

with $\Delta = \Delta_r + \frac{1}{r^2}\frac{\partial^2}{\partial\theta^2}$ the Laplacian operator in cylindrical coordinates. Note however that the problem has now lost its radial symmetry. A particular solution of this equation is $h_p(\mid \mathbf{r}-\mathbf{r}_1 \mid)+h_\mathrm{p}(\mid \mathbf{r}-\mathbf{r}_2 \mid)$, the function h_p being given by (22). The general solution of the biharmonic equation $\Delta\Delta h = 0$ that satisfies the requirement $\lim_{r\to\infty}\Delta h = 0$ with a finite value at the origin is simply a constant. If we impose the conditions $h(\mathbf{r}_1) = h(\mathbf{r}_2) = 0$, we are led to the solution of the differential equation (25)

$$h(\mathbf{r}) = h_\mathrm{p}(\mid \mathbf{r}-\mathbf{r}_1 \mid)+h_\mathrm{p}(\mid \mathbf{r}-\mathbf{r}_2 \mid)-h_\mathrm{p}(l)-h_\mathrm{p}(0) \quad (26)$$

with l the distance between polymers, $l = \mid \mathbf{r_1}-\mathbf{r_2} \mid$. The interaction potential $V(l)$ is given by the difference between the free energy (24) and twice the free energy of one isolated polymer. Inserting the solution of the Euler-Lagrange equation in (24) and integrating by parts leads to

$$V_\mathrm{curv}(l) = -\kappa\int \mathrm{d}S\Delta h_\mathrm{p}(\mathbf{r})\Delta h_\mathrm{p}(\mathbf{r}-\mathbf{l}). \quad (27)$$

The potential $V(l)$ is always negative: the membrane-mediated interaction between two polymers attached on the same side of the bilayer is attractive. It also follows from equation (27) that two polymers anchored to *the opposite side of a membrane* repel each other. The interaction potential has in this case the same functional form but with the reverse sign. The interaction potential is shown in Figure 4 for two polymers grafted on the same side. Notice that the potential range is of the order of the polymer size: at larger distances, the deformation field having a zero curvature shape, the cost of grafting a second polymer to it is the same as grafting a polymer to a flat interface. The mechanisms responsible for attraction or repulsion are easy to understand. When two polymers are grafted to the *same side* of a membrane, they can both share the same deformation profile, instead of creating each one a profile of their own. When they are grafted to *opposite sides*, the deformations are mutually neutralized: the polymers can only fully develop their deformation profiles at a large distance from each other.

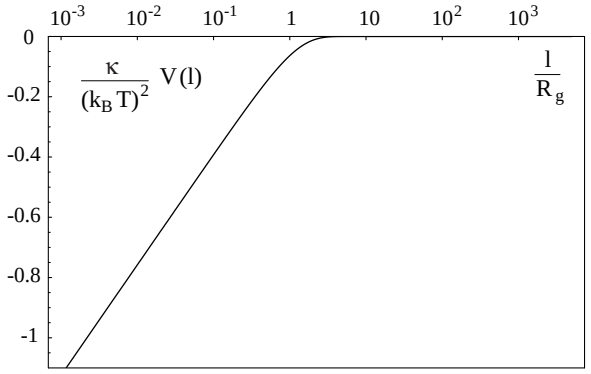

Fig. 4. The membrane-mediated interaction potential between two Gaussian polymers, grafted to the same side of a membrane. Polymers grafted on opposite sides have the same functional form with the reverse sign.

At short distances ($l \ll R_\mathrm{g}$), the attraction has a logarithmic behaviour:

$$V_\mathrm{curv}(l) \simeq \frac{(k_\mathrm{B}T)^2}{2\pi\kappa}\ln(l/R_\mathrm{g}). \quad (28)$$

For soft membranes the elastic constant is of order $k_\mathrm{B}T$, which leads, for a polymer with a radius of gyration of ten nanometers, $R_\mathrm{g} = 10$ nm and a minimum approaching distance of the order of a monomer size $l = 0.3$ nm, to an attraction well of a couple of $k_\mathrm{B}T$. Moreover, the potential varies quadratically with temperature, this class of interactions is thus quite sensitive to temperature variations. We will further discuss in the conclusions the possible implications of such sensitivity.

It is important to stress the differences between the potential that we just described and other membrane-induced interactions abundantly described recently [30, 31]. The pressure patches do not lead to Casimir-like interactions, there are here no logharitmic or algebraic tails. In the literature, the inclusions are considered as rigid bodies that set the value of the membrane curvature at the inclusion site. It can be checked that our case corresponds to "local" curvature source of imposed *strength*, that does not lead to long-range interactions. On the contrary, if the curvature sources fix the local curvature *amplitude*, then long-range interactions will arise [32]. In the jargon of membrane-induced interactions, our potential corresponds

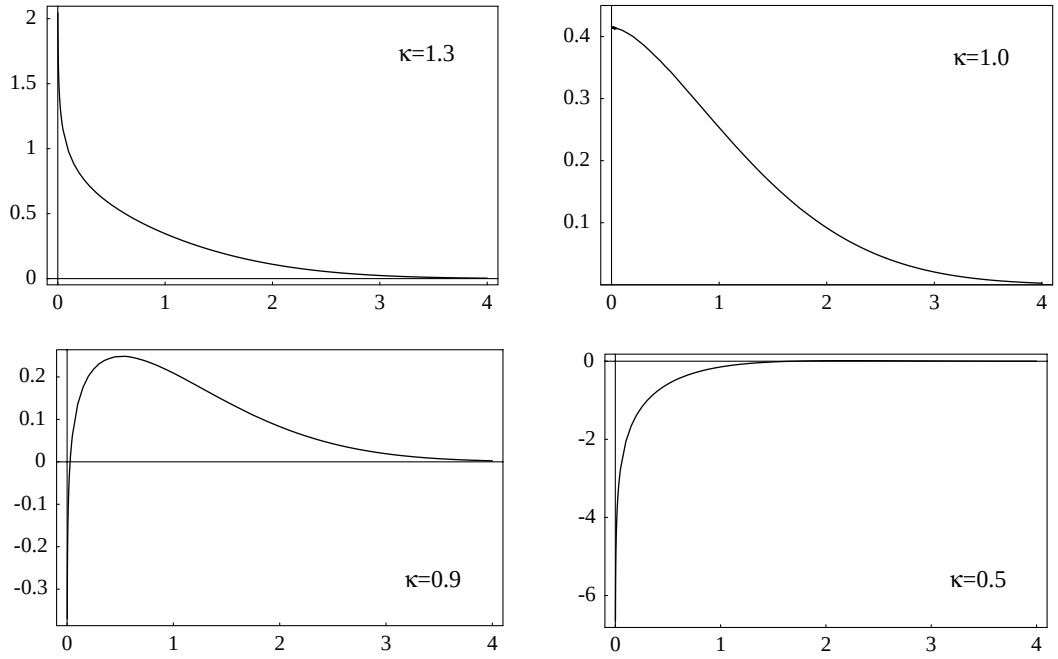

Fig. 5. The two-body interaction potential with the estimated inter-chain repulsion. The plots show $\frac{2\pi V(l)}{k_{\rm B}T}$ as a function of $l/R_{\rm g}$ for different values of the bending rigidity (in $k_{\rm B}T$ units), with fixed parameter $b = 1/(2\pi)$.

to a "short range" potential. Notice however that for polymers, the range of the interaction can be at least one order of magnitude larger ($\sim$ tens of nanometers) than typical inclusion sizes ($\sim$ few nanometers).

The potential (27) accounts only for curvature-mediated interactions. At distances of order $R_{\rm g}$, inter-chain interactions give also rise to a repulsive contribution. We qualitatively account for the polymer-polymer repulsion by separating the two chains with a mid-plane hard wall [24]. This over-estimated repulsive potential reads $-k_{\rm B}T\ln[\mathrm{erf}(l/R_{\rm g})]$. We now write the total interaction potential as

$$V(l) = V_{\rm curv}(l) - b\,k_{\rm B}T\ln[\mathrm{erf}(l/R_{\rm g})] \qquad (29)$$

with b a constant smaller than unity. Both parts behave logarithmically at short distances: the potential is attractive for small values of the bending rigidity and is repulsive for high values. Figure 5 shows the plots of $V(l)$ for different values of the rigidity κ and b arbitrarily fixed at $b = 1/(2\pi)$. In this paticular case the crossover between attraction and repulsion occurs at $\kappa = k_{\rm B}T$. Changing the value of b will accordingly rescale the crossover value. When the surface is covered with a finite density of chains, the onset of aggregation can be monitored by the second virial coefficient B:

$$B = \frac{1}{2}\int \mathrm{d}S\left(1 - \exp\left\{-\frac{V(\mathbf{r})}{k_{\rm B}T}\right\}\right). \qquad (30)$$

The plot of B as a function of the bending rigidity with our particular choice of b is shown in Figure 6: for $\kappa < 0.6k_{\rm B}T$, the second virial coefficient becomes negative, indicating aggregation of different chains.

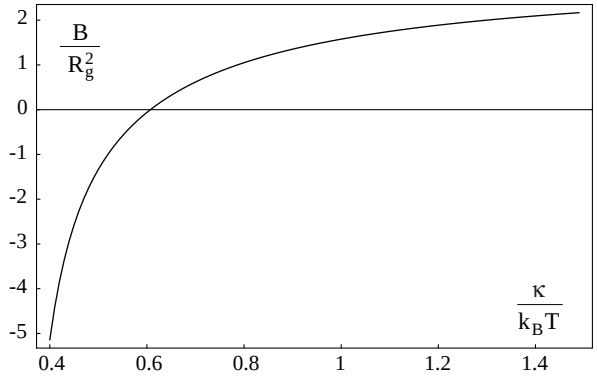

Fig. 6. The second virial coefficient as a function of the bending rigidity (in $k_{\rm B}T$ units), with fixed paramater $b = 1/(2\pi)$. Chains aggregation is induced by negative B, which occurs at $\kappa < 0.6k_{\rm B}T$ for this particular value of b.

3.3 Star-like polymer aggregates

Attractive interactions between chains grafted to the surface may lead to a star-like structure: the grafting points merge into a core, while excluded volume repulsions acting on the arms give the aggregate the hemispherical shape displayed in Figure 7. We now discuss how the structure of the aggregate changes the nature of the pressure applied to the grafting surface, and the deformation that the pressure induces on a free-standing elastic membrane.

The structure of a star polymer with f arms of polymerization index N can be described by the Daoud-Cotton model [33]. Attachment of the chains to a central core effectively forces the local polymer density to be everywhere inside the star above overlapping concentration. The star

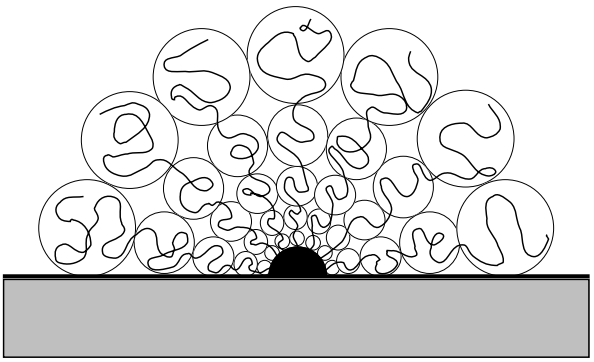

Fig. 7. The conformation of a star anchored to a plane. Inside each "blob" of size $\xi(r) \sim rf^{-1/2}$ the branches have a single-chain behaviour.

can therefore be described as a semi-dilute solution [20], with a local, position-dependent screening length $\xi(r)$, where r is here the distance from the center of the star in a frame of spherical coordinates. Pictorially, we represent this by associating with each arm a string of blobs of increasing size $\xi(r)$. The radial dependence of the blob size $\xi(r)$ can be obtained by noticing that at a distance r from the center there are f blobs of cross-section $\xi(r)^2$ occupying a total area of $4\pi r^2$. The blob size thus varies as $\xi(r) \simeq rf^{-1/2}$ and the corresponding local polymer concentration as $c_{\rm s}(r) \simeq f^{2/3}a^{-5/3}r^{-4/3}$. Note that there is a crowded region of size $R_{\rm c} \simeq af^{1/2}$ in the middle of the star where the concentration reaches one. The size of the star can be obtained from monomer conservation $Nf = 4\pi \int_0^R r^2 {\rm d}r c_{\rm s}(r)$. Neglecting the small-core region one gets $R \simeq aN^{3/5}f^{1/5}$.

The structure of interest to us is a half-star, simply obtained from the Daoud and Cotton model by replacing $f/2$ arms by a repulsive half-plane —see Figure 7. The local pressure is a simple function of the blob size $p_{\rm s}(r) \sim k_{\rm B}T\xi(r)^{-3}$, leading to a pressure applied *on the surface* of the form

$$p_{\rm s}(r) \simeq f^{3/2}\frac{k_{\rm B}T}{r^3}\ , \tag{31}$$

where r is the distance from the center in a surface cylindrical frame. The reasons beyond this functional form can also be related to the interfacial structure of the star. Close to the surface there is a monomer depletion layer, growing from the surface as $c(r,z) \sim z^{5/3}$. Due to screening, the bulk behaviour is recovered when one crosses the cone surface $z = rf^{-1/2}$, which correspond to the first blob layer [34]. Writing again the r-dependence of the depletion layer such as to match the bulk value $c_{\rm s}(r) \simeq f^{2/3}a^{-5/3}r^{-4/3}$, one gets $c(r,z) \simeq p_{\rm s}(r)(z/a)^{5/3}$, with $p_{\rm s}(r)$ the pressure field in equation (31). For distances r larger than the star size, we expect the pressure to vanish rapidly.

For ideal chains, the pressure applied by f chains grafted at the same point is f times larger than the pressure applied by a single chain. For polymers with excluded volume there is an additional crowding effect that results in a pressure $f^{3/2}$ times larger than the pressure of a single chain. Also, the range of the pressure grows as the star size, and is a factor $f^{1/5}$ larger than the range of a single chain. Since the pressure field close to the grafting point has the same scaling form as a single-chain pressure, the patch still induces a conic deformation on a free-standing elastic membrane. The angle of the cone is more pronounced for a star than the angle of a pinch from a single chain

$$h_{\rm s}(r) \simeq -f^{3/2}\left(\frac{k_{\rm B}T}{\kappa}\right)r \tag{32}$$

and the energy gained by the creation of the star-pinch is much greater than the the sum of the energy gains of f individual pinches

$$\frac{F_{\rm curv}}{k_{\rm B}T} \sim -\frac{k_{\rm B}T}{\kappa}f^3\ln\left(\frac{R}{a}\right). \tag{33}$$

The Daoud-Cotton model also allows to compute the excluded-volume cost to build a star-like structure, the result is

$$\frac{F_{\rm ev}}{k_{\rm B}T} \sim f^{3/2}\ln\left(\frac{R}{a}\right). \tag{34}$$

For a number of chains f greater than a threshold $f_0 \sim (\kappa/k_{\rm B}T)^{2/3}$, aggregation is always favored. Nevertheless, that process might be slow since it is hindered by an energy barrier $\Delta F \sim \kappa$. It is also important to stress that the mecanical constraints on the bilayer may limit the maximum aggregation number. This can be determined by setting $\mid \nabla h \mid \sim 1$ in expression (32) which leads to $f_{\rm max} \sim f_0$. At this stage a piece of membrane decorated with $f_{\rm max}$ polymers might as well detach from the main membrane, leading to a coexistence between decorated membranes and decorated small vesicles or micelles [7].

4 Polymers anchored on a constrained membrane

In most practical situations, the bilayer does not stand free in the solvent but it is subjected to additional constraints. In this section, we consider two important situations. First we discuss the pressure applied by a grafted polymer to a supported bilayer. Supported bilayers are fluid membranes that adhere to a substrate, allowing for instance for the observation of cell phenomena like membrane protein aggregation, opening of ionic channels and others [35–37]. Adhesion of membranes on a substrate plays a role in biological phenomena such as endocytosis and exocytosis [2]; it is also of relevance in biotechnological processes, such as drug delivery by liposomes [38]. A second important case of constraint membranes corresponds to lamellar L_α phases, where the membranes are confined by interactions with their neighbors in the lamella stack [4,39].

4.1 Supported bilayers

We consider a membrane adhering to a flat surface with a contact energy per unit area $\Gamma/2$. The combined effect

of the polymer pressure and the point-like anchoring force peels off a region of radius L and central height $h_0 = h(r = 0)$. The corresponding free energy functional is

$$F[h(r), L, h_0] = F_0 - \Gamma\pi L^2 + \frac{\kappa}{2}\int_0^L 2\pi r\mathrm{d}r(\Delta_r h)^2 + \int_0^L 2\pi r\mathrm{d}r p(r)(h(r) - h_0) \quad (35)$$

with F_0 a constant. Notice that the membrane height h is here measured with respect to the substrate. Performing the functional minimization of equation (35) with respect to the deformation h leads to an Euler-Lagrange differential equation identical to equation (20) of the free-standing case, with boundary conditions $h(0) = h_0$, $h(L) = 0$ and $\frac{\mathrm{d}h}{\mathrm{d}r}(L) = 0$. Further minimization of the free energy (35) with respect to the size of the peeled region L, and with respect to the height at the origin h_0, provides two more boundary conditions :

$$\frac{\partial F}{\partial L} = 0 \Leftrightarrow \Delta h(r = L) = \left(\frac{\Gamma}{\kappa}\right)^{1/2}, \quad (36)$$

$$\frac{\partial F}{\partial h_0} = 0 \Leftrightarrow \frac{\mathrm{d}}{\mathrm{d}r}\Delta h(r = L) = 0. \quad (37)$$

Relation (36) equates the balance between the attractive potential and the elastic moment at the contact line $r = L$ [40]. The peeled radius is given by the implicit equation for L,

$$\frac{1}{4}\exp\left(-\frac{L^2}{4R_\mathrm{g}^2}\right) - \frac{\sqrt{\pi}}{2}\frac{R_\mathrm{g}}{L}\mathrm{erf}\left(\frac{L}{2R_\mathrm{g}}\right) + \pi\frac{L}{R_\mathrm{g}}\beta = 0. \quad (38)$$

The parameter $\beta^2 = \kappa\Gamma R_\mathrm{g}^2/(k_\mathrm{B}T)^2$ controls the value of L. For small adhesive energies or very flexible membranes we have $\beta \ll 1$, the membrane is loosely attached to the surface and the deformation is similar to the free-standing case: $L = R_\mathrm{g}/(2\sqrt{\pi}\beta)^{1/2}$ and $h_0 = (k_\mathrm{B}T/4\sqrt{\pi}\kappa)R_\mathrm{g}\ln(L/R_\mathrm{g})$. For large adhesive energies or stiff membranes, $\beta \gg 1$, only the conical deformation survives and the pinch height is proportional to the peeled radius: $L = R_\mathrm{g}/(2\pi\beta)$ and $h_0 = (3k_\mathrm{B}T/16\pi\kappa)L$. One might be astonished that these quantities cannot be expressed only as a function of the length $\lambda_0 = (\kappa/\Gamma)^{1/2}$. For many problems involving bending energies and adhesion (or interfacial tension) of membranes this length separates two regimes. On length scales larger than λ_0, adhesion or tension effects dominate the behaviour of the membrane, while for lengths below λ_0 the deformation is ruled by the bending curvature. In our case, the results can also be understood in terms of λ_0, by recalling first the simpler case of a membrane that adheres to the surface but has a fixed, given height ζ_0 at the origin. It is easy to show that in that case the peeling radius is given by $L = (8\lambda_0^2\zeta_0^2)^{1/4} \sim (\lambda_0\zeta_0)^{1/2}$. But when a polymer patch is applied, the height is fixed by the polymer pressure and it follows, for strong adhesions, the conic form (21). One has thus $\zeta_0 \sim L/\kappa$ which leads to $L \sim \lambda/\kappa$. This holds up to a length L of the order of the radius of gyration R_g. For smaller adhesion strengths the balance is determined by $\zeta_0 \sim R_\mathrm{g}/\kappa$ leading to $L \sim (R_\mathrm{g}\lambda_0/\kappa)^{1/2}$.

Adhesion energies can be found in the range $\Gamma \sim 10^{-7}$–10^{-4} N · m^{-1} [41]. For typical bending moduli $\kappa \sim 5$–$20k_\mathrm{B}T$, the extension of the peeled zones is in the range of one to ten nanometers, which is also the typical size for polymers.

4.2 Membrane in a potential well

In this section, we focus on the effect of pressure patches applied to membranes confined in an harmonic potential. This is for instance relevant to describe the lyotropic smectic phases L_α [12] but serves also as a paradigm for other situations where the membrane is constraint by an external soft potential. The energy functional of one bilayer reads

$$F[h(r)] = F[0] + \int_0^\infty 2\pi r\mathrm{d}r p(r)(h(r) - h_0) + \frac{\kappa}{2}\int_0^\infty 2\pi r\mathrm{d}r(\Delta_r h)^2 + \frac{B}{2}\int_0^\infty 2\pi r\mathrm{d}r h(r)^2, \quad (39)$$

where h_0 is the value of the deformation at the origin. In the case of a stack of membranes the amplitude of the harmonic potential B is the compression modulus of the system and can be related to the curvature of the interaction potential. The natural length arising in expression (39) is $l_0 = (\frac{\kappa}{B})^{1/4}$. On scales larger than l_0 the deformation is controlled by the harmonic potential while on smaller scales the behaviour of the membrane is ruled by curvature effects. In particular, for non-ionic L_α phases where steric Helfrich interactions control the repulsion between the membranes [42,43], it is possible to show that the lenght l_0 is proportional to the average interlamellar spacing d

$$l_0 = (\frac{\pi}{6})^{1/2}(\frac{\kappa}{k_\mathrm{B}T})^{1/2}d \quad (40)$$

Minimizing the free energy functional with respect to $\zeta = h - h_0$ leads to

$$\kappa\Delta_r\Delta_r\zeta(r) + B\zeta(r) = -(p(r) + Bh_0) \quad (41)$$

with boundary conditions $\zeta(0) = 0$ and $\zeta(\infty) = -h_0$. In order to solve equation (41), we first evaluate the associated Green function $g(r, r')$ defined by

$$\kappa\Delta_r\Delta_r g(r, r') + Bg(r, r') = \delta(r - r') \quad (42)$$

so that the deformation field ζ is eventually obtained from

$$\zeta(r) = -\int_0^\infty \mathrm{d}r' g(r, r')(p(r) + Bh_0). \quad (43)$$

A straightforward but tedious calculation gives for $r > r'$

$$g_+(r, r') = -\frac{k_\mathrm{B}T}{\kappa}l_0^2 r'\{\mathrm{Bei}_0(r'/l_0)\mathrm{Ker}_0(r/l_0) + \mathrm{Ber}_0(r'/l_0)\mathrm{Kei}_0(r/l_0) + \frac{4}{\pi}\mathrm{Kei}_0(r'/l_0)\mathrm{Kei}_0(r/l_0)\} \quad (44)$$

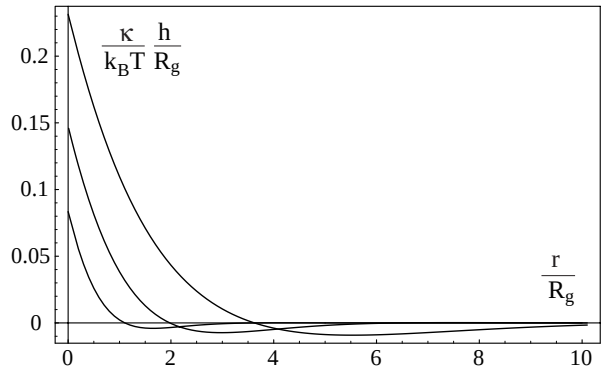

Fig. 8. The deformation profile of a fluid membrane for different strengths of the harmonic potential. The curves are plotted for $\alpha = 0.5$, 1 and 2, the largest deformation corresponding to the weaker potential.

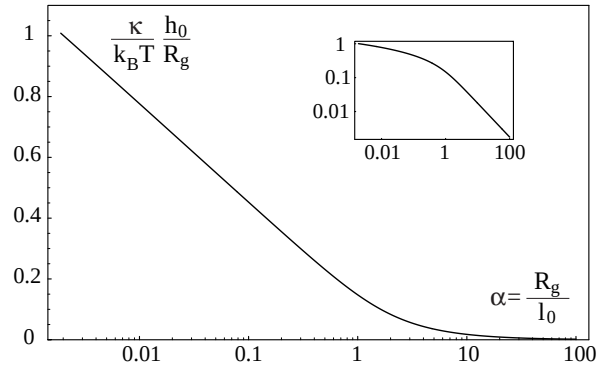

Fig. 9. Amplitude of the pinch at the grafting point. The parameter α controls the strength of the potential. For a soft potential, h_0 varies like the logarithm of α. The insert emphasizes the scaling form for large values of α.

and for $r < r'$

$$g_-(r,r') = -\frac{k_{\rm B}T}{\kappa} l_0^2 r' \{ {\rm Bei}_0(r/l_0){\rm Ker}_0(r'/l_0) + {\rm Ber}_0(r/l_0){\rm Kei}_0(r'/l_0) + \frac{4}{\pi}{\rm Kei}_0(r/l_0){\rm Kei}_0(r'/l_0)\}, \quad (45)$$

where the Kelvin functions ${\rm Ber}_0(x)$, ${\rm Bei}_0(x)$, ${\rm Ker}_0(x)$ and ${\rm Kei}_0(x)$ are the real and imaginary parts of the modified Bessel functions ${\rm I}_0(xe^{i\pi/4})$ and ${\rm K}_0(xe^{i\pi/4})$ [23]. The harmonic potential allows then for an oscillatory profile, as depicted in Figure 8.

The amplitude of the deformation, h_0 is obtained by minimizing the free energy with respect to h_0, leading to

$$h_0 = l_0 \frac{k_{\rm B}T}{8\kappa} \int_0^\infty \frac{{\rm d}x}{x^2} \left(1 + \frac{4}{\pi}{\rm Kei}_0(x)\right) \times \exp\left(-\frac{x^2}{4\alpha^2}\right)\left(1 + \frac{x^2}{2\alpha^2}\right), \quad (46)$$

where $\alpha = R_{\rm g}/l_0$. Asymptotically h_0 varies like the logarithm of α for small values of α, and decays with a power law for large values: $h_0 \sim \alpha^{-2}$ —see Figure 9. For Helfrich systems where the length l_0 is proportional to the interlamellar spacing $l_0 \sim d$ (and $\kappa \sim k_{\rm B}T$), one may easily induce a deformation of $0.1d$, by using polymers of gyration radius $R_{\rm g} \sim 0.5d$. For even smaller polymers the amplitude of the deformation becomes comparable to the polymer size. For polymers much larger than the interlamellar distances, our approach would need to be completed by accounting also for the pressure exerted by the polymer on the neighboring membranes (of order of $k_{\rm B}Td^{-3}$) [44].

5 Discussion and conclusion

We have developed in this paper a new picture to describe the interactions between a grafted polymer and a flexible membrane.

We have shown that the polymer behaves in fact as a *small pressure tool*. The pressure applied by this tool is very high close to the grafting point and decays sharply over a distance of order $R_{\rm g}$, the gyration radius of the chain. Through scaling arguments and numerical simulations we further confirmed that excluded-volume interactions mainly change the range of the pressure field, while its amplitude and functional form are rather independent of solvent conditions.

Under the pressure of the polymer, a flexible interface assumes a characteristic deformation: each flexible surface is a pressure sensor. We have shown that for fluid membranes, the deformation has a pinched conic form. The exact shape of the pinch depends on the boundary conditions imposed upon the membrane, but its form at the center of the deformation field is rather universal.

For many grafted polymers, the deformation field induces an interaction potential between the polymers. We have shown that this potential is attractive for polymers grafted on the same side of a membrane and repulsive for polymers grafted on opposite sides. This interaction potential rises interesting possibilities. For instance, by changing the temperature one might expect to control the aggregation behavior of polymers grafted on the membrane. Also, if many polymers are added to a vesicle, the attraction might bring many polymers to the same site, increasingly catastrophically the pressure until a decorated micelle or small vesicle detaches from the surface.

Our treatment of the polymer-induced deformations does not account for the fluctuations of the membrane. Thermal fluctuations arise spontaneously in membrane systems on the scales above the de Gennes-Taupin persistence length: $\xi = a' \exp(\frac{4\pi\kappa}{k_{\rm B}T})$ [45]. When the elastic constants are of the order of $k_{\rm B}T$, the lenght ξ is in the range 10–100 nm, and fluctuations become important. At the level of the first-order perturbation scheme implemented in this paper, the pressure is an external field that couples only linearly to the deformation of the membrane, so the fluctuation spectrum is not perturbed. It is therefore important to extend to second order this type of perturbative expansion in order to determine both the corrections to the elastic parameters of the membrane and the corrections to the fluctuation spectrum itself.

We gratefully aknowledge inspiring discussions with L. Auvray, J.-B. Fournier, S. Obukov and T.A. Witten.

References

1. J.N. Israelachvili, *Intermolecular and Surface Forces* (Academic Press, New York, 1992).
2. B. Alberts, D. Bray, A. Johnson, J. Lewis, M. Raff, K. Roberts, P. Walter, *Molecular Biology of the Cell* (Garland Publishing, New York, 1998).
3. J.C. van de Pas, *Coll. Surf. A* **85**, 221 (1994).
4. H.E. Warriner, S.H.J. Idziak, N.L. Slack, P. Davidson, C.R. Safinya, *Science* **271**, 969 (1996).
5. Y. Yang, R. Prudhomme, K.M. McGrath, P. Richetti, C.M. Marques, *Phys. Rev. Lett.* **80**, 2729 (1998).
6. G. Bouglet, C. Ligoure, A.-M. Bellocq, E. Dufourc, G. Mosser, *Phys. Rev. E* **57**, 834 (1998).
7. R. Joannic, L. Auvray, D.D. Lasic, *Phys. Rev. Lett.* **78**, 3402 (1997).
8. H. Ringsdorf, J. Venzmer, F. Winnik, *Angew. Chem. Int. Ed. Engl.* **30**, 315 (1991).
9. M.E. Cates, *Nature* **351**, 102 (1991).
10. V. Frette, I. Tsafir, M.-A. Guedeau-Boudeville, L. Jullien, D. Kandel, J. Stavans, *Phys. Rev. Lett.* **83**, 2465 (1999).
11. P.B. Canham, *J. Theor. Biol.* **26**, 61 (1970); W. Helfrich, *Z. Naturforsch.* **28c**, 693 (1973).
12. S. Safran, *Statistical Thermodynamics of Surfaces, Interfaces and Membranes* (Addison-Wesley, Reading, Mass., 1994).
13. R. Cantor, *Macromolecules* **14**, 1186 (1981).
14. S.T. Milner, T.A. Witten, M.E. Cates, *Macromolecules* **22**, 853 (1989).
15. R. Podgornik, *Europhys. Lett.* **21**, 245 (1993).
16. R. Lipowsky, *Europhys. Lett.* **30**, 197 (1995).
17. A. Hanke, E. Eisenriegler, S. Dietrich, *Phys. Rev. E* **59**, 6853 (1999).
18. T. Bickel, C. Jeppesen, C.M. Marques, *Phys. Rev. E* **62**, 1124 (2000).
19. During the preparation of this manuscript, an independent work by M. Breidenich, R.R. Netz, R. Lipowsky appeared in *Europhys. Lett.* **49**, 431 (2000), describing some of the results presented in our paper.
20. P.-G. de Gennes, *Scaling Concepts in Polymers Physics* (Cornell University Press, Ithaca, New York, 1979).
21. E. Eisenriegler, *Polymers Near Surfaces* (World Scientific, Singapore, 1993).
22. M. Doi, S.F. Edwards, *The Theory of Polymer Dynamics* (Clarendon Press, Oxford, 1986).
23. M. Abramowitz, I.A. Stegun, *Handbook of Mathematical Functions* (National Bureau of Standards, Washington, DC, 1964).
24. C.M. Marques, J.-B. Fournier, *Europhys. Lett.* **35**, 361 (1996).
25. G. Barton, *Elements of Green's Functions and Propagation* (Clarendon Press, Oxford, 1989).
26. C. Hiergeist, R. Lipowsky, *J. Phys. II* **6**, 1465 (1996).
27. E. Eisenriegler, *Phys. Rev. E* **55**, 3116 (1997).
28. K. Kremer, in *Computer Simulations in Chemical Physics*, edited by M.P. Allen, D.J. Tildesley (Kluwer Academic Publishers, 1993), pp. 397-459.
29. P.G. Dommersnes, J.-B. Fournier, *Eur. Phys. J. B* **12**, 9 (1999).
30. M. Goulian, R. Bruinsma, P. Pincus, *Europhys. Lett.* **22**, 145 (1993).
31. P.G. Dommersnes, J.-B. Fournier, P. Galatola, *Europhys. Lett.* **42**, 233 (1998).
32. J.-B. Fournier, private communication. In practice this can be checked by adding a $\alpha\Delta h$ term at point $\mathbf{r}_1$ and $\mathbf{r}_2$ and computing the membrane free energy as a function of $\mid \mathbf{r}_1 - \mathbf{r}_2 \mid$. If α is a constant, then the interaction vanishes. See also P.G. Dommersnes, J.-B. Fournier, *Eur. Phys. J. B.* **12**, 9 (1999).
33. M. Daoud, J. Cotton, *J. Phys. (Paris)* **43**, 531 (1982).
34. In this picture, only the first blob layer is perturbed. Despite the breaking down of the spherical symmetry near the wall, our approach is still valid: while replacing half of the star by a wall, the interactions are still of order $k_{\mathrm{B}}T$ per blob.
35. U. Seifert, R. Lipowsky, *Phys. Rev. A* **42**, 4768 (1990).
36. A. Albersdörfer, R. Bruinsma, E. Sackmann, *Europhys. Lett.* **42**, 227 (1998).
37. A.-L. Bernard, M.-A. Guedeau-Boudeville, L. Jullien, J.-M. DiMeglio, *Europhys. Lett.* **46**, 101 (1999).
38. D.D. Lasic, *Tibtech* **16**, 307 (1998).
39. F. Castro-Roman, G. Porte, C. Ligoure, *Phys. Rev. Lett.* **82**, 109 (1999).
40. L.D. Landau, E.M. Lifshitz, *Theory of Elasticity* (Butterworth-Heinemann, Oxford, 1998).
41. U. Seifert, *Adv. Phys.* **46**, 13 (1997).
42. W. Helfrich, *Z. Naturforsch.* **33a**, 305 (1978).
43. C.R. Safinya, D. Roux, G.S. Smith, S.K. Sinha, P. Dimon, N.A. Clarck, A.-M. Bellocq, *Phys. Rev. Lett.* **57**, 2718 (1986).
44. T. Bickel, C. Jeppesen, C.M. Marques, *C. R. Acad. Sci. IIb (Paris)* **328**, 661 (2000).
45. P.-G. de Gennes, C. Taupin, *J. Phys. Chem.* **88**, 2294 (1982).